nature neuroscience

Activation of raphe nuclei triggers rapid and distinct effects on parallel olfactory bulb output channels

Vikrant Kapoor[1–3], Allison C Provost[1–3], Prateek Agarwal[1,2] & Venkatesh N Murthy[1,2]

The serotonergic raphe nuclei are involved in regulating brain states over timescales of minutes and hours. We examined more rapid effects of raphe activation on two classes of principal neurons in the mouse olfactory bulb, mitral and tufted cells, which send olfactory information to distinct targets. Brief stimulation of the raphe nuclei led to excitation of tufted cells at rest and potentiation of their odor responses. While mitral cells at rest were also excited by raphe activation, their odor responses were bidirectionally modulated, leading to improved pattern separation of odors. *In vitro* whole-cell recordings revealed that specific optogenetic activation of raphe axons affected bulbar neurons through dual release of serotonin and glutamate. Therefore, the raphe nuclei, in addition to their role in neuromodulation of brain states, are also involved in fast, sub-second top-down modulation similar to cortical feedback. This modulation can selectively and differentially sensitize or decorrelate distinct output channels.

Information processing in the brain is modulated by the state of the animal. Endogenous neuromodulators such as serotonin (5-hydroxytryptamine or 5-HT), acetylcholine and norepinephrine are differentially released in a state-dependent manner and alter the function of neural circuits by modifying the properties of neurons and synapses[1,2]. The serotonergic system is of particular interest because it has been linked to a wide variety of brain functions[3–12]. 5-HT is released by neuronal populations in raphe nuclei in the brainstem, which project throughout the brain[11] and activate a wide range of signaling pathways in a diverse array of neurons[11,13].

Although most studies on the serotonergic system have focused on the timescale of mood (hours to days), raphe neuron activity can also be modulated at sub-second time scales[5,14,15], allowing it to have a dynamic impact on ongoing behavior. Earlier studies have examined serotonergic modulation using exogenous application of agonists[6,8,9,16]. Recent advances in optogenetics allow the study of fast and direct effects of transmitter release from raphe axons, allowing spatial and temporal specificity. Furthermore, one can also investigate the role of neurotransmitters other than 5-HT that are potentially released by raphe axons, particularly glutamate[5,17,18].

The serotonergic system is thought to modulate sensory processing[8], including that in the olfactory system[6,9], but the exact nature of such modulation remains unclear. The olfactory bulb (OB) receives odor information from the nose and is the first synaptic processing station in the olfactory system[19]. Incoming information is processed by several types of neurons and sent to multiple brain regions via the axons of mitral and tufted cells (MCs and TCs)[19,20]. TCs and MCs project to divergent downstream targets and carry distinct information[19,21,22]. The raphe nuclei send dense projections to the olfactory bulb (OB)[23,24] and can affect incoming information at the first synapse in the input layer[9]. *In vitro*, 5-HT can excite external tufted cells (ETCs)[25] and can elicit both inhibition and excitation in MCs[26]. How activation of the raphe nuclei affects information leaving the OB under native conditions has remained unknown. Here we have used optogenetics, optophysiology and electrophysiology to investigate how the activation of the raphe nuclei modulates the OB output at fast times scales *in vivo*. In particular, since the activity of neurons in raphe nuclei can fluctuate with behavior over sub-second time scales[5,14,15,27], we set out to explore how brief increases in the activity of raphe neurons can alter early olfactory processing.

RESULTS

Modulation of OB principal neurons at rest

We imaged, using multiphoton microscopy, the responses of MCs and TCs to brief activation of the raphe (**Fig. 1**). MCs and TCs were labeled with calcium indicator GCaMP6s (ref. 28) in the Tbx21-Cre (T-box 21, also called Tbet) mouse line[29], in which Cre recombinase is specifically and exclusively expressed in principal cells of the OB. The indicator was expressed by injection of AAV2.9 virus carrying GCaMP6s into the OBs of Tbx21-Cre mice (see Online Methods and **Supplementary Fig. 1**). Two to 6 weeks after virus injection, mice were anesthetized and cranial windows were placed over the hindbrain and over the OBs (to image TCs and MCs). Placement of the stimulating electrode (see Online Methods) was validated with *post hoc* histology (**Fig. 1a**). The *in vivo* experiments were performed in anesthetized mice unless stated otherwise.

Since the raphe nuclei are known to be involved in the regulation of breathing[12], we first examined whether the breathing rate was altered by brief stimulation of raphe. At the stimulation parameters used for the experiments in this study (three 1-ms pulses at 10 Hz), no change in breathing rate was apparent (**Fig. 1b**,**c**). This indicates that modulation of MCs and TCs in our experiments was not caused by changes in breathing rate, which could alter how odors are sampled by mice and the dynamics of OB circuits[30].

We identified TCs and MCs (**Fig. 1d**,**g**) on the basis of the depth at which their somata were located and their morphology (see Online

[1]Center for Brain Science, Harvard University, Cambridge, Massachusetts, USA. [2]Department of Molecular & Cellular Biology, Harvard University, Cambridge, Massachusetts, USA. [3]These authors contributed equally to this work. Correspondence should be addressed to V.K. (vkapoor@mcb.harvard.edu) or V.N.M. (vnmurthy@fas.harvard.edu).

Received 3 September 2015; accepted 30 November 2015; published online 11 January 2016; doi:10.1038/nn.4129

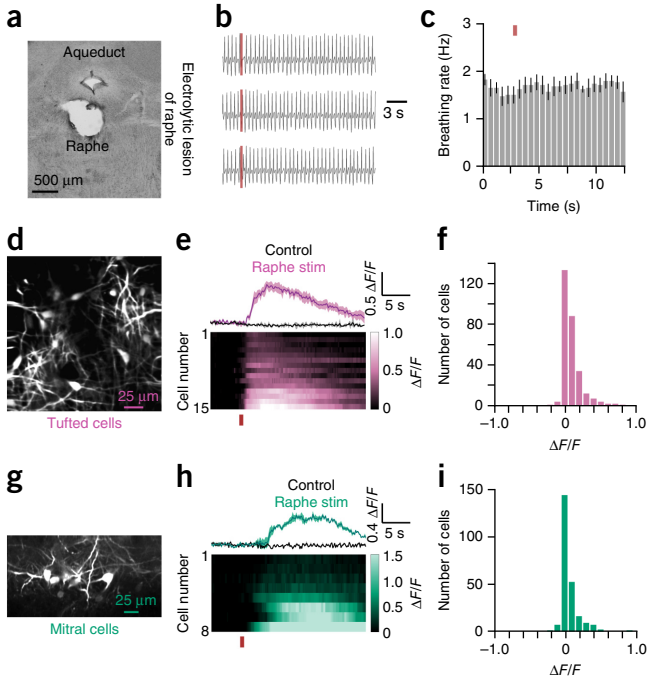

Figure 1 Raphe stimulation excites mitral and tufted cells at rest. (**a**) Histological section showing an electrolytic lesion in the raphe nucleus introduced with the stimulating electrode at the end of an experiment. (**b**) Three exemplar trials showing breathing traces measured with a chest strap around the time of raphe stimulation (three 1-ms pulses at 10 Hz; red vertical bars). Upward deflections correspond to inhalation. (**c**) Peristimulus time histogram (PSTH) of breathing rate across 5 animals. Red bar denotes time of raphe stimulation and black lines are s.e.m. (**d**) Resting fluorescence image of TCs in an exemplar experiment shown in **e**. (**e**) Average trace showing TC response to raphe activation (purple). Time course of fractional fluorescence intensity for all cells in the field of view in **d** in response to raphe activation (red bar). Cell 15 is plotted at top. (**f**) Bar plot of all imaged TCs showing fluorescence change in trials with raphe stimulation when compared to blank trials with no raphe stimulation (288 cells, 12 mice, $P = 9.80 \times 10^{-29}$, Wilcoxon signed-rank). (**g**) Resting fluorescence image of MCs in one experiment, analyzed in **h**,**i**. (**h**) Average trace showing an example MC responding to activation of raphe (teal green). Time course of fractional fluorescence intensity for all cells in the field of view in **g** in response to raphe activation (red bar). Cell 7 is plotted at top. (**i**) Bar plot of fluorescence changes in all imaged MCs for trials with raphe stimulation compared to blank trials with no stimulation (238 cells, 13 mice, $P = 4.68 \times 10^{-10}$, Wilcoxon signed-rank).

Methods and **Supplementary Fig. 1**). Brief stimulation of raphe evoked robust, repeatable excitation in single TCs from rest (**Fig. 1e**) and across a population of TCs (**Fig. 1f**). Although the excitation was large in many cells, other cells in the same region were not affected by raphe activation. The average fractional fluorescence increase was 7.2 ± 0.72% (s.e.m.; **Fig. 1f**; 288 cells from 12 animals, median change of 2.87%), which was significantly different from zero ($P = 9.80 \times 10^{-29}$, Wilcoxon signed-rank).

We next examined the effects of raphe stimulation on MCs (**Fig. 1g**). Many, but not all, MCs were excited by brief raphe activation (**Fig. 1h**). The average fractional fluorescence increase in MCs was 5.1 ± 0.91% (**Fig. 1i**; 238 cells from 13 animals, median change of 2.24%), which was significantly different from zero ($P = 4.68 \times 10^{-10}$, Wilcoxon signed-rank) and also significantly lower than that in TCs ($P = 3.6 \times 10^{-5}$, Wilcoxon rank-sum). These results indicate that brief stimulation of raphe leads to fast excitation in both TCs and MCs at rest, which was surprising given the prior expectation of slow effects by neuromodulatory systems.

Modulation of TC odor responses

Since raphe stimulation excited TCs at rest, we hypothesized that this excitation would affect odor responses. To test this hypothesis, we imaged odor-evoked responses in TCs (**Fig. 2a**,**b**) with and without raphe stimulation (three 1-ms pulses at 10 Hz delivered 1 s into odor presentation). Two to 6 odors were chosen from a panel of 25 odors (**Supplementary Fig. 2**) on the basis of a quick screen of responses for the collection of imaged cells in each experiment. Odors typically elicited fluorescence increases in TCs (**Fig. 2b**,**c**), which tended to be of larger amplitude when paired with raphe activation (**Fig. 2b**,**c**). We rank ordered each cell's odor tuning profile on the basis of the average odor response in the absence of raphe stimulation and then compared them to the odor tuning profile with raphe activation (**Fig. 2d**). Results from an exemplar experiment for 62 cells and 6 odors illustrate that there is an overall enhancement of odor responses with raphe stimulation (**Fig. 2c**,**d**). To quantify the effects of raphe modulation further, we calculated the number of odors to which individual cells responded under different experimental conditions. Within-cell comparison indicated that TCs generally responded to more odors with raphe stimulation (**Fig. 2e**; mean change of 2.4 ± 0.06 and median increase of 2 odors; significantly different from zero, $P = 7.50 \times 10^{-13}$, Wilcoxon signed-rank). These results indicate that the tuning widths of TCs, which

Figure 2 TC odor responses are sensitized by raphe inputs. (**a**) Two-photon image showing resting fluorescence of GCaMP6s in TCs. (**b**) Time course of fluorescence responses of two TCs to raphe stimulation (black), odor stimulation (light green) and raphe and odor stimulation (purple). Bars denote odor timing (light green) and raphe stimulation timing (red). Error bars are s.e.m. (**c**) Time course of responses to 6 odors in 62 TCs in the imaged region shown in **a**. Light green and red bars at bottom indicate the timing of the odor and raphe stimulation, respectively. (**d**) Heat map representing the double rank-ordered odor responses without (light green) and with (purple) raphe activation. Each row indicates the odor response amplitudes of single cells ($n = 62$), with the rows themselves rank ordered in increasing amplitude of responses (summed across all odors). The order of cells was determined in the left panel and was maintained for the right panel (with raphe stimulation) for direct comparison. Bar plots on the right show the normalized summed activity of single cells and bar plots at the bottom show normalized summed activity for odors. Hex, hexanal; PA, propyl acetate; ET, ethyl tiglate; EV, ethyl valerate; MT, methyl tiglate; Val, valeraldehyde. (**e**) Top, bar plot showing the change in the number of odors that elicited responses without and with raphe stimulation for cells shown in **c** (372 cell–odor pairs, $P = 7.50 \times 10^{-13}$, Wilcoxon signed-rank). Bottom, bar plot showing the change in the number of odors that elicited responses without and with raphe stimulation for all cell–odor pairs from 6 animals (1,087 cell–odor pairs, $P = 1.68 \times 10^{-10}$, Wilcoxon signed-rank). (**f**) Top, cumulative distribution of the change in fluorescence for TCs without raphe stimulation (light green) or with raphe stimulation (purple) for all cell–odor pairs shown in **c** and **d**. Bottom, same for TCs without (black) or with raphe stimulation (purple) for all cell–odor pairs ($n = 1087$) across 6 animals. (**g**) Scatter plots showing change in odor response for each TC when the raphe is stimulated (compared to odor response on its own), as a function of raphe response (left) and odor response (right) for that TC. Each dot is a single cell–odor pair. (**h**) Three-dimensional scatter plot showing the responses for TCs (372 cell–odor pairs) for odor and raphe stimulation. The prediction surface, shown as a grid, is from the interaction-based regression model (see Online Methods). (**i**) Scatter plot showing predictions based on the interactive model versus observed responses for odor and raphe stimulation from an exemplar animal (372 cell–odor pairs). Colors depict different odors; $R^2 = 0.88$. (**j**) Scatter plot showing the predicted versus observed responses for odor and raphe stimulation. Colors depict different animals; $R^2 = 0.86$ ($n = 6$ animals, 1,087 cell–odor pairs, $P = 1.29 \times 10^{-21}$, F test).

are broad to begin with[31,32], tend to be further broadened by raphe activation. The enhancement in odor responses (916 of 1087 cell–odor pairs showed significant increase; see Online Methods) and increase in the number of odors eliciting responses were robust (**Fig. 2e**) and consistent across experiments (**Fig. 2e**,**f**, bottom; mean change of 2.9 ± 0.04 and median increase of 3 odors, 6 animals, significantly different from 0, $P = 1.68 \times 10^{-10}$, Wilcoxon signed-rank).

We observed notable diversity in the effects of raphe stimulation on the odor responses of TCs (**Fig. 2b**,**c**,**g**). Odor responses were differentially modulated in different TCs, (**Fig. 2b**,**c**,**g**), and even in the same cell raphe stimulation had distinct effects on responses to different odors (**Fig. 2b–d** and **Supplementary Fig. 3**). We next asked what might predict the TC odor responses in the presence of raphe stimulation by performing four different types of regression analysis on the data (see Online Methods). Neither raphe responses nor odor responses in isolation predicted TC responses to concurrent odor and raphe stimulation ($R^2 = 0.10$ and $R^2 = 0.66$ respectively for raphe and odor stimulation, **Fig. 2g**), but a linear regression model using

both raphe and odor responses as variables performed much better (R^2 = 0.79). Furthermore, a regression model that also included a term for interaction between the raphe and odor responses (interactive regression model) performed the best (R^2 = 0.88; **Fig. 2h**). The four-parameter fit was better than the three parameter fit according to goodness of fit measures ($P = 1.29 \times 10^{-21}$, F test, **Supplementary Fig. 3**). We also found that this predictive model was consistent across odors (**Fig. 2i**), as well across animals (**Fig. 2j**).

Previous experiments indicated that strong electrical stimulation of the raphe reduce odor-evoked responses in olfactory sensory axons (OSNs)[9]. Using a mouse line in which the genetically encoded calcium indicator GCaMP3 is expressed exclusively in OSNs, we found that brief stimulation of the raphe (three 1-ms pulses at 10 Hz) did not alter odor-evoked responses in the sensory inputs (**Supplementary Fig. 4**). These data suggest that raphe inputs to the OB provide a means of sensitizing TCs, increasing the probability of TCs responding to odors and also enhancing existing odor responses of TCs.

Modulation of MC odor responses

We next explored how MC odor responses are modulated by raphe activation using GCaMP6s to image their odor-evoked responses (**Fig. 3a**,**b**). Surprisingly, MC odor responses could be both suppressed and enhanced by raphe activation (**Fig. 3b**,**c**; 770 of 1,050 cell–odor pairs showed significant modulation; see Online Methods). The double rank-ordered plots indicate that some odor responses increased while others decreased, and that this was not stereotyped within a cell (**Fig. 3d**) or within an odor. Notably, pairwise comparison of individual MCs with and without raphe activation indicated a broad range of changes, including both increase and decrease in the number of odors that evoke responses (**Fig. 3e**, top), but with no systematic change across the population (**Fig. 3e**; mean change in the number of odors was 0.1 ± 0.08 and median change of 0, not significantly different from 0, P = 0.61 for n = 47 cells, Wilcoxon signed-rank) and these results were consistent across animals (**Fig. 3e**, mean change in the number of odors was 0.0 ± 0.04, median change of 0, not significantly different from 0, P = 0.85 for 1,050 cells from 7 animals, Wilcoxon signed-rank). In contrast to TCs (**Fig. 2e**,**f**), the number of odors that activated a given MC was the same, on average, with and without raphe activation (**Fig. 3e**), and there was no systematic increase in the responses of MCs (**Fig. 3f**; P = 0.9 for 1,050 cells from 7 animals, Wilcoxon signed-rank). The bidirectional nature of MC modulation is, therefore, distinct from the pattern of TC modulation.

The modulation of MCs showed remarkable diversity (**Fig. 3g**), dependent on the cell identity as well as odor identity. We asked whether the regression analysis we performed for TCs would also be able to predict MC enhancement or suppression. We found that even the interactive model was poor at predicting the modulation of MC odor responses in presence of raphe stimulation (**Fig. 3h**). These data indicate that MC odor responses are bidirectionally modulated by brief raphe activation, and this modulation is dissimilar to that measured in TCs.

Selective stimulation of raphe axons

The effects reported above involved electrical stimulation of the raphe nucleus. To confirm that these effects were due to specific excitation of the raphe nuclei, we turned to a transgenic mouse line (TPH2-ChR2-YFP) in which channelrhodopsin-2 (ChR2) is expressed specifically in serotonergic neurons[33]. These neurons and axons can be selectively activated using light stimulation in the raphe or the OB. We confirmed that raphe projections were found throughout the different layers of the OB using the fluorescence of YFP, which is coexpressed with ChR2 (**Fig. 4a** and **Supplementary Fig. 5**).

We recorded from single putative MCs or TCs (M/TCs) on the dorsal surface of the OB using tungsten electrodes and stimulated raphe axons with blue light (three 10-ms pulses at 10 Hz, 15 mW/mm^2 of power). Brief and specific activation of raphe fibers increased the firing rates in the recorded units (**Fig. 4b,c**; n = 17 units). This excitation was not due to nonspecific effects such as light-induced heating, since none of the 8 cells recorded from wild-type animals were significantly modulated (data not shown).

To compare the optical and electrical stimulation more directly, we recorded from M/TCs as described above and also inserted a bipolar stimulating electrode into raphe nucleus. Fast excitation was elicited by both optogenetic activation and electrical stimulation (**Fig. 4d**, left), although the time courses differed. Notably, 3 of the 9 cells that were significantly modulated by electrical activation of raphe were also significantly modulated by optogenetic stimulation (**Fig. 4d**, right). On average, the firing rate increased 20-fold (± 12) and 40-fold (± 28) from baseline, with optogenetic stimulation and electrical stimulation, respectively.

To further characterize the effects of optical stimulation of the raphe on OB principal neurons, we labeled neurons in the OB with GCaMP6s using a nonconditional AAV2.9 virus injected in TPH2-ChR2 mice (see Online Methods). This strategy led to labeling of many cell types in the OB, with fewer labeled TCs and MCs than when using the flex virus in Tbx21-Cre animals, but these principal cells could be readily identified on the basis of their morphology and depth. To stimulate raphe neurons optically, we implanted an optical fiber in the raphe nucleus of these animals (see Online Methods). We imaged the activity of both MCs and TCs during optogenetic activation of raphe, with and without odor stimulation (**Fig. 4e**,**h**). As with electrical stimulation (**Fig. 2c**), we found that the TC odor responses were potentiated by brief raphe activation (**Fig. 4e–g**; 96 of 144 cell–odor pairs from 3 animals showed significant potentiation), with a mean change of 27.53 ± 2.3% ($P = 1.2 \times 10^{-23}$, Wilcoxon signed-rank test, median change of 20.82%), whereas the modulation in MC odor responses was bidirectional (41 of 64 cell–odor pairs from 2 animals showed significant modulation; **Fig. 4h–j**; mean 1.69 ± 3.9% and median change of 1.29%; see Online Methods). These data suggest that the distinct modulatory effects on the two principal neuronal populations of the OB are due to specific activation of serotonergic neurons in the raphe.

Activation of raphe axons modulates TC activity *in vitro*

The distinct and differential modulation of TC and MC network prompted us to explore the cellular and synaptic mechanisms underlying these effects using acute OB slices and whole-cell patch-clamp recordings[34]. We first measured synaptic responses of TCs to raphe inputs in slices from the TPH2-ChR2-YFP mouse. A patch pipette was targeted to TCs in the external plexiform layer (**Fig. 5a**), and excitatory and inhibitory currents were recorded under voltage clamp at −70 mV and 0 mV, respectively.

Blue light stimulation (three 10-ms pulses at 10 Hz) elicited both inhibitory and excitatory currents in TCs (**Fig. 5b**). Excitatory and inhibitory currents were asynchronous and lasted for hundreds of milliseconds (**Fig. 5b**, right). We quantified both excitatory and inhibitory events by calculating the total charge transferred at −70 mV and 0 mV (**Fig. 5c**,**d**). Excitatory events were initiated quickly and inhibitory events were delayed, as judged by the time points at which the light-stimulated traces diverge from control traces (**Fig. 5c**). Targeted raphe fiber stimulation increased excitatory charge by 0.0287 ± 0.003 nC (median change of 0.0277 nC and $P = 3.1 \times 10^{-27}$ for 6 cells from 4 animals, Wilcoxon signed-rank test) and inhibitory charge

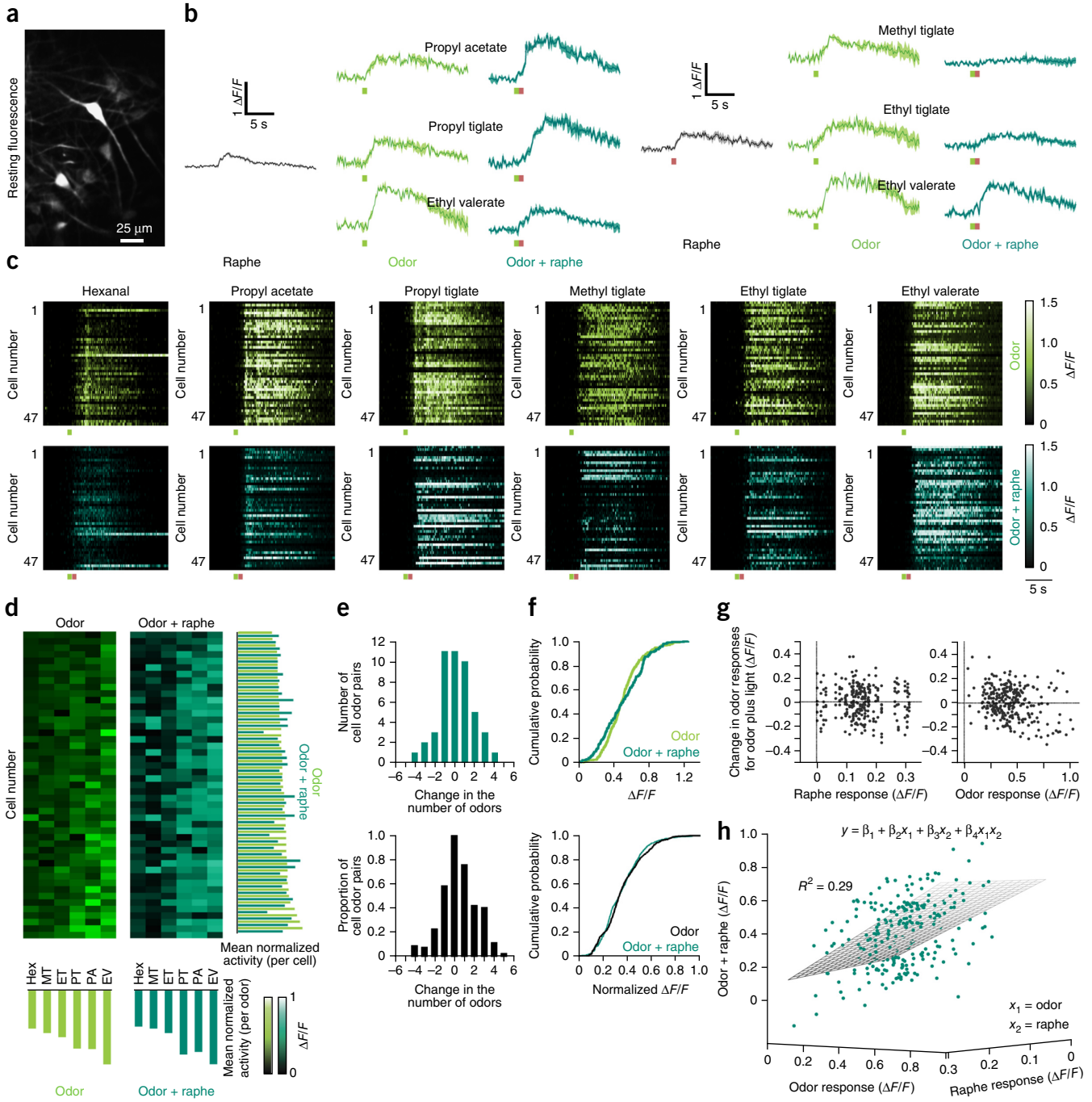

Figure 3 MC odor responses are bidirectionally modulated by raphe inputs. (**a**) Two-photon image showing resting fluorescence of GCaMP6s in MCs. (**b**) Time courses of fluorescence of two MCs in response to raphe stimulation (black), odor stimulation (light green) and raphe and odor stimulation (teal green). Bars are odor timing (light green) and raphe stimulation timing (red). Error bars are s.e.m. (**c**) Time course of responses to 6 odors in 47 MCs in the imaged region. Green and red bars at bottom indicate the timing of the odor and raphe stimulation, respectively. (**d**) Heat map representing the double rank-ordered odor responses without (light green) and with (teal green) raphe activation. Each row indicates the odor response amplitudes of single cells ($n = 47$), with the rows themselves rank ordered in increasing amplitude of responses (summed across all odors). The order of cells was determined in the left panel and was maintained for the right panel (with raphe stimulation) for direct comparison. Bar plots on the right show the normalized summed activity of single cells and bar plots at the bottom show normalized summed activity for odors; abbreviations as in **Figure 2**. (**e**) Top, bar plot showing the change in the number of odors that elicited responses without and with raphe stimulation for cells shown in **c** ($P = 0.61$ for $n = 47$ cells, Wilcoxon signed-rank). Bottom, bar plot showing the change in the number of odors that elicited responses without and with raphe stimulation for all cell–odor pairs ($P = 0.85$ for 1,050 cells from 7 animals, Wilcoxon signed-rank). (**f**) Top, cumulative distribution of the change in fluorescence for MCs without (light green) or with (teal green) raphe stimulation for all cell–odor pairs shown in **c** and **d**. Bottom, cumulative distribution of the change in fluorescence for MCs without raphe stimulation (black) or with raphe stimulation (teal green) for all the cell–odor pairs ($n = 1,050$) across 7 animals. (**g**) Scatter plots showing change in odor response for each MC when the raphe is stimulated (compared to odor response on its own), as a function of raphe response (left) and odor response (right) for that MC. Each dot is a single cell–odor pair. (**h**) Three-dimensional scatter plot showing the responses for MCs (282 cell–odor pairs) for odor and raphe stimulation ($R^2 = 0.29$). Grid shows the prediction manifold based on the interaction-based regression model (see Online Methods).

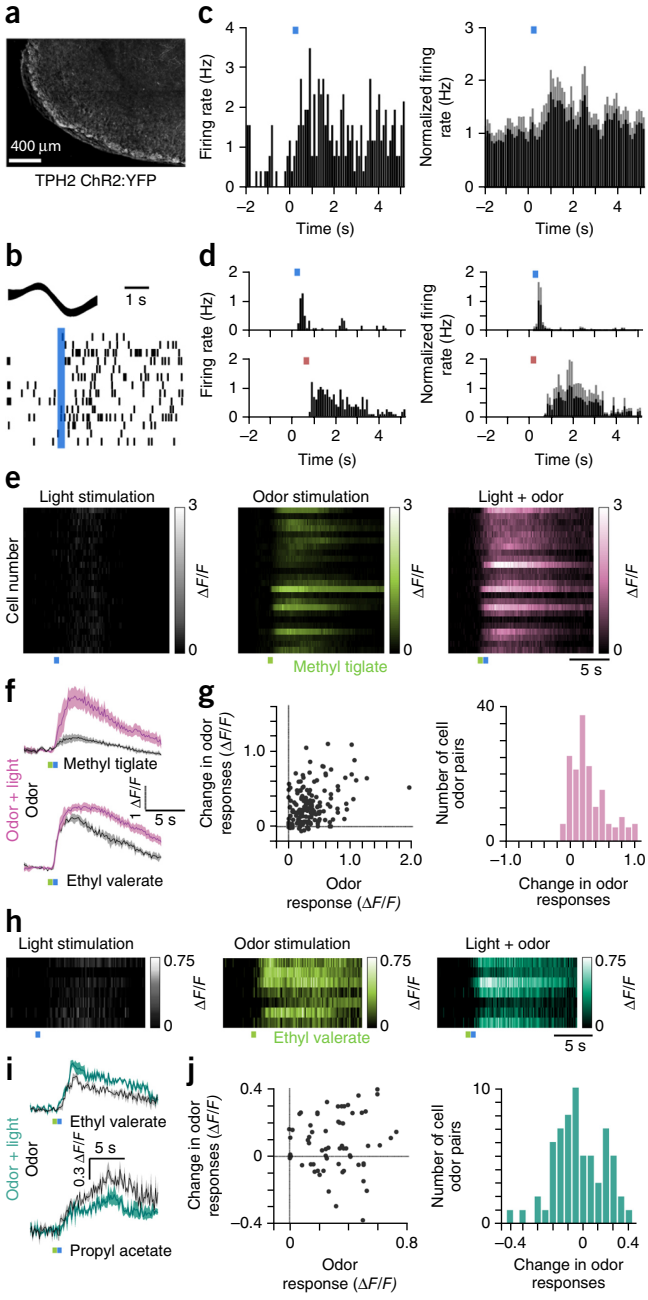

Figure 4 Optogenetic activation of raphe leads to excitation of principal cells. (**a**) Confocal image of the raphe fibers innervating different layers of the OB in a TPH2-ChR2:YFP mouse. (**b**) Extracellular spikes from an isolated unit (820 spikes superimposed at top) recorded in the OB are represented in a raster plot (bottom). Twenty trials of dorsal surface stimulation with blue light (timing indicated by blue bar). (**c**) PSTH of activity of a single putative M/TC (left) in the TPH2-ChR2:YFP mouse exhibiting excitation from rest when raphe fibers are activated via blue light (100-ms bins, same for all PSTHs). Population PSTH of all putative M/TCs (right) from extracellular recordings in the TPH2-ChR2:YFP mouse ($n = 17$ cells). Gray shading indicates s.e.m. (**d**) Left, PSTH of activity in a single putative M/TC in the TPH2-ChR2:YFP mouse reveals excitatory responses to blue light stimulation (top; timing indicated by the blue bar) and electrical stimulation of the raphe (bottom; timing indicated by red bar). Right, population PSTH of all putative M/TCs both with electrical stimulation (bottom) and ChR2 stimulation (top) in the TPH2-ChR2:YFP mouse ($n = 9$ cells). Firing rate in the resting period for each cell was normalized before averaging, and the final average was normalized to the peak for clarity of display. (**e**) Time course of responses in 24 TCs in 3 animals for light stimulation (gray, left), odor stimulation (light green, middle; methyl tiglate) and odor plus light stimulation (purple, right). Light green and blue bars at bottom indicate the timing of the odor and ChR2 stimulation, respectively. (**f**) Time courses of fluorescence changes in a single TC in response to odor stimulation alone (black) and odor stimulation plus light stimulation of raphe (purple) for two different odors. Shading indicates s.e.m. (**g**) Left, scatter plot showing change in odor responses caused by concurrent raphe stimulation as a function of odor response. Right, bar graph showing distribution of changes in odor responses in TCs caused by optical stimulation of the raphe for 144 cell–odor pairs from 3 animals ($P = 1.2 \times 10^{-23}$, Wilcoxon signed-rank test). (**h**) Time course of responses in 7 MCs from 2 animals for light stimulation (gray), odor stimulation (light green, ethyl valerate) and odor plus light stimulation (teal green). Light green and blue bars at bottom indicate the timing of the odor and ChR2 stimulation, respectively. (**i**) Time courses of fluorescence changes in a single MC in response to odor stimulation alone (black) and odor stimulation plus light stimulation of raphe (teal green) for two different odors. Shading indicates s.e.m. (**j**) Left, scatter plot showing change in odor responses in MCs caused by concurrent raphe stimulation, as a function of odor response. Right, bar graph showing distribution of changes in odor responses in MCs caused by optical stimulation of the raphe for 64 cell–odor pairs from 2 animals (right).

by 0.41 ± 0.08 nC (median change of 0.4128 nC and $P = 3.3 \times 10^{-3}$, Wilcoxon signed-rank test, $n = 6$ cells).

We used pharmacological manipulations to uncover the molecular basis of light-evoked responses in TCs. Surprisingly, methysergide (50 µM), a broad-spectrum 5-HT receptor antagonist, led to increased excitation onto TCs (143.82 ± 2.52% of the no-drug control, $P = 5.01 \times 10^{-4}$, Wilcoxon rank-sum test, $n = 8$ cells; **Fig. 5e**, left), rather than blocking the effect. Methysergide also reduced light-evoked inhibitory currents measured at 0 mV (70.83 ± 14.76% of no-drug control, $P = 3.92 \times 10^{-3}$, Wilcoxon rank-sum test, $n = 8$ cells; **Fig. 5e**, right). By contrast, raphe excitation onto TCs was blocked by ionotropic glutamate receptor blockers (50 µM AP5 and 20 µM CNQX, $P = 7.61 \times 10^{-29}$, Wilcoxon rank-sum test, $n = 7$ cells; **Fig. 5e**) and part of the inhibition was also blocked by these drugs (39.10 ± 5.31% of no-drug control, $P = 2.10 \times 10^{-7}$, Wilcoxon rank-sum test, $n = 7$ cells; **Fig. 5e**). Together, these results suggest that both glutamate and 5-HT release contribute to the modulation of electrical activity in TCs. Light-induced TC excitation was increased by application of a $GABA_A$ receptor blocker, 20 µM gabazine (128.74 ± 9.68% of no-drug control, $P = 2.0 \times 10^{-3}$, Wilcoxon rank-sum test, $n = 6$ cells; **Fig. 5e**), and inhibition was blocked (2.58 ± 1.30% of no-drug control, $P = 1.92 \times 10^{-21}$, Wilcoxon rank-sum test, $n = 6$ cells; **Fig. 5e**).

To explore the effect of raphe axon activation on the spiking activity of TCs, we recorded from TCs in current-clamp mode (**Fig. 5f**) and promoted spike firing by injecting different amounts of current while probing with blue light 500 ms after the onset of the current step. TC firing rates were potentiated by light stimulation across all current injections (**Fig. 5g,h**; 50.15 ± 8.95%, $P = 1.21 \times 10^{-3}$, Wilcoxon rank-sum test, $n = 5$ cells), mimicking the potentiation in odor responses recorded *in vivo* (**Fig. 2b**). Potentiation of TC firing rate was blocked by ionotropic glutamate receptor blockers (50 µM AP5 and 20 µM CNQX, $P = 1.43 \times 10^{-8}$, Wilcoxon rank-sum test, $n = 5$ cells; **Fig. 5g,h**), which also uncovered an inhibitory modulation by raphe axons (**Fig. 5g,h**; −8.01 ± 4% in presence of AP5 and CNQX compared to no-drug control, $P = 1.43 \times 10^{-8}$, Wilcoxon rank-sum test, $n = 5$ cells). Notably, blocking 5-HT receptors (116.15 ± 15% of no-drug control, $P = 0.072$, $n = 5$ cells) or $GABA_A$ receptors (133.60 ± 14.10% of no-drug control, $P = 0.068$, $n = 5$ cells; **Fig. 5g,h**) increased the degree of potentiation. Firing rates also increased for TCs at rest (4.38 ± 0.48 Hz, $P = 9.21 \times 10^{-3}$, Wilcoxon rank-sum test, $n = 5$ cells; **Fig. 5f,g**), which

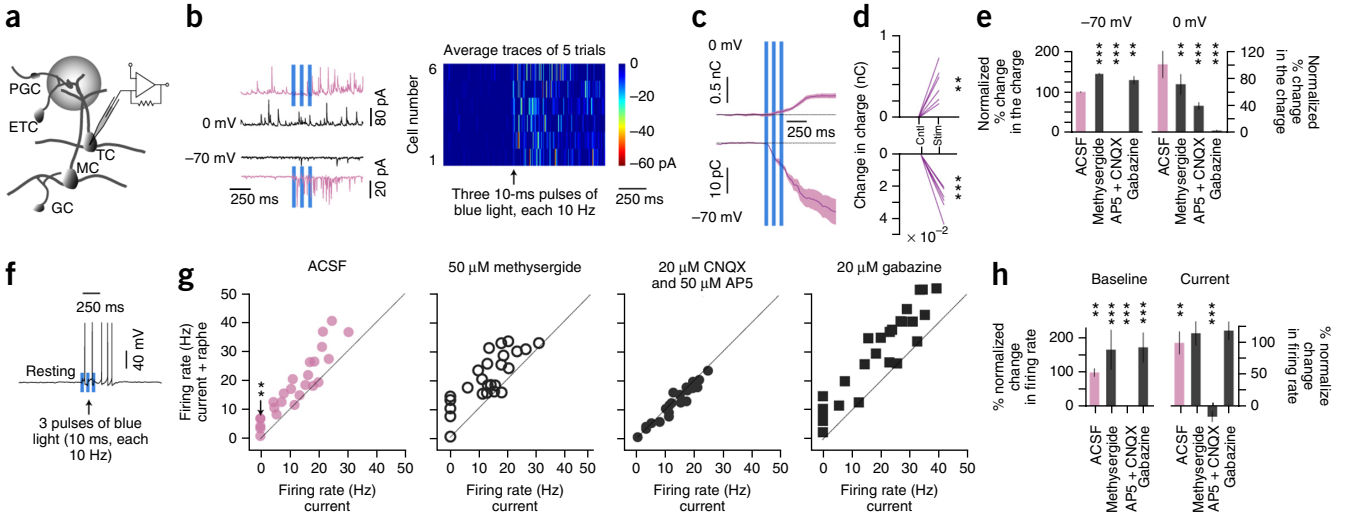

Figure 5 Modulation of TCs by optogenetic activation of raphe projections in main olfactory bulb slices. (**a**) Diagram depicting TC recordings from OB slices. PGC: periglomerular cell, GC: granule cell. (**b**) Left, whole-cell voltage-clamp recordings from a TC at 0 mV and −70 mV showing inhibitory postsynaptic currents (IPSCs) (top) and EPSCs (bottom) with (purple) and without (black) raphe fiber activation. Blue bars depict the timing of raphe fiber activation. Right, average time series for six TCs showing EPSCs elicited by brief optogenetic activation of raphe fibers (black arrow). (**c**) Bottom, integrated charge transfer in a TC at −70 mV with (purple) optogenetic activation of raphe fibers. Top, change in integrated charge transfer at 0 mV with (purple) optogenetic activation of raphe fibers. (**d**) Summary of all six recorded TCs, showing increase in both inhibitory charge transfer (top, $P = 3.1 \times 10^{-27}$ for 6 cells from 4 animals, Wilcoxon signed-rank test) and excitatory charge transfer (bottom, $P = 3.3 \times 10^{-3}$, Wilcoxon signed-rank test, $n = 6$ cells from 4 animals) by light stimulation. Cntl, control; Stim, stimulation. (**e**) Normalized light-induced percentage change in charge transfer from baseline for EPSCs (left, −70 mV) and IPSCs (right, 0 mV) in presence of 5-HT receptor antagonist (50 μM methysergide, $P = 5.01 \times 10^{-4}$ and $P = 3.92 \times 10^{-3}$ for excitatory and inhibitory charge transfer respectively, Wilcoxon rank-sum test, $n = 8$ cells from 5 animals), glutamate receptor antagonists (20 μM CNQX and 50 μM AP5, $P = 7.61 \times 10^{-29}$ and 2.10×10^{-7} for excitatory and inhibitory charge transfer, respectively, Wilcoxon rank-sum test, $n = 7$ cells from 5 animals) and GABA receptor antagonist (20 μM gabazine, $P = 2.0 \times 10^{-3}$ and $P = 1.92 \times 10^{-21}$ for excitatory and inhibitory charge transfer respectively, Wilcoxon rank-sum test, $n = 6$ cells from 6 animals). Data for some conditions are not visible since they are close to 0. (**f**) Example trace of a TC recorded under current clamp showing spikes in response to raphe fibers activation. Blue bars indicate blue light timing. (**g**) Scatter plots comparing the firing rate of TCs for different step current injection with and without serotonergic fiber activation without drug (ACSF, $P = 1.21 \times 10^{-3}$, Wilcoxon rank-sum test, $n = 5$ cells from 5 animals) or with glutamate receptor antagonists (20 μM CNQX and 50 μM AP5, $P = 1.43 \times 10^{-8}$, Wilcoxon rank-sum test, $n = 5$ cells from 5 animals), 5-HT receptor antagonist (50 μM methysergide, $P = 0.072$, $n = 5$ cells from 3 animals, Wilcoxon rank-sum test) and GABA receptor antagonist (20 μM gabazine, $P = 0.068$, $n = 5$ cells from 4 animals, Wilcoxon rank-sum test). Firing rates calculated for an 800 ms period starting at the time of first light stimulation. (**h**) Light-triggered changes in firing rates of TCs for no current injection (left, $P = 9.21 \times 10^{-3}$, Wilcoxon rank-sum test, $n = 5$ cells from 4 animals) and averaged across all (excluding zero) levels of current injection (right). The changes for different pharmacological manipulations were normalized to the condition with no drugs applied (ACSF). $^{**}P < 0.01$ and $^{***}P < 0.001$. Error bars represent s.e.m.

was similar to the effect of raphe stimulation on basal fluorescence of TCs *in vivo* (**Fig. 1d–f**). This excitation was blocked by AP5 and CNQX ($P = 1.44 \times 10^{-6}$, Wilcoxon rank-sum test, $n = 5$ cells; **Fig. 5h**), but was increased by both methysergide and gabazine (168.91 ± 56.21% and 173.45 ± 43.81% compared to no-drug control, respectively; $P = 2.74 \times 10^{-4}$ and 1.90×10^{-5}, respectively; Wilcoxon rank-sum test, $n = 5$ cells; **Fig. 5h**).

Together, these data indicate that optogenetic activation of raphe axons elicited large excitatory currents in TCs both at rest and when they were active. In addition to this excitation primarily driven by glutamate, there was an inhibitory component driven through 5-HT receptors and local GABAergic circuits in the OB.

Activation of raphe axons modulates MC activity *in vitro*

We next asked how raphe modulation of MC firing compares with that of TCs by recording from MCs *in vitro* (**Fig. 6a,b**). As in our *in vivo* results (**Fig. 1g–i**), MCs were activated from rest by light (**Fig. 6c**; increase of 10.01 ± 3.32 Hz, $P = 2.0 \times 10^{-3}$, Wilcoxon rank-sum test, $n = 7$ cells from 4 animals), but were bidirectionally modulated by light when they were induced to fire spikes through current injection (**Fig. 6b,c**). This effect contrasts with that on TCs, which were uniformly potentiated by light stimulation of raphe axons (**Fig. 5g**). Individual MCs could be either potentiated or inhibited, and there was no systematic dependence on firing rate (**Fig. 6b**). Furthermore, we found that the excitation-to-inhibition ratio (see Online Methods) for MCs varied significantly more (**Fig. 6d,e**) than that of TCs (mean 0.08 and 0.11 and s.d. 0.065 and 0.092 for TCs and MCs respectively).

Application of methysergide largely blocked the inhibitory MC modulation (**Fig. 6f**), resulting in an overall potentiation of firing rate (201.58 ± 9.20% of the no-drug condition, $P = 1.1 \times 10^{-19}$, Wilcoxon rank-sum test, $n = 5$ cells from 3 animals; **Fig. 6g**). Conversely, application of AP5 and CNQX blocked the excitatory effect (**Fig. 6f**), with a net reduction of firing rate (−29.88 ± 15.42% of no-drug condition, $P = 7.2 \times 10^{-31}$, Wilcoxon rank-sum test, $n = 5$ cells; **Fig. 6g**). This indicates that, as measured in TCs, 5-HT had an inhibitory effect, while glutamate was responsible for the excitatory effect. In fact, 5-HT appears to have a greater inhibitory effect in MCs (**Fig. 6g**) than TCs (**Fig. 5h**, right). Some of the inhibitory effects were also mediated by $GABA_A$ receptors, as gabazine increased the firing rates (147.14 ± 11.38% of no-drug control, $P = 8.79 \times 10^{-3}$, Wilcoxon rank-sum test, $n = 5$ cells; **Fig. 6f,g**). MC recordings *in vitro* strongly corroborated the effects on MC odor responses observed *in vivo* (**Fig. 3b,c**), with single MCs *in vitro* exhibiting both excitation and inhibition of their firing rates. Whether modulation was excitatory or inhibitory depended on firing

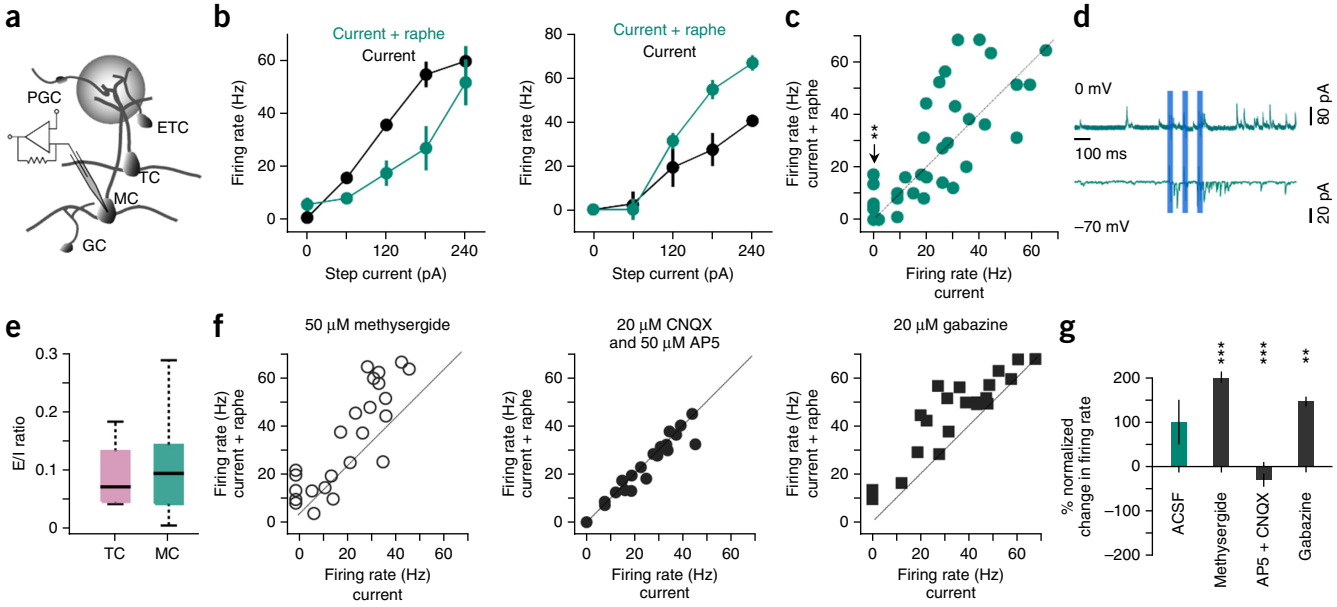

Figure 6 Modulation of MC activity by optogenetic activation of raphe fibers. (**a**) Diagram depicting MC recordings from OB slices. (**b**) Plot of the relationship between injected current and firing rate for two different MCs showing both inhibitory and excitatory effects of raphe fiber activation. (**c**) Scatter plots comparing the firing rate of MCs for different step current injection with and without raphe fiber activation. Arrow points to trials where light stimulation induced firing in MCs that were quiescent ($P = 2.0 \times 10^{-3}$, Wilcoxon rank-sum test, $n = 7$ cells from 4 animals). $^{**}P < 0.01$. (**d**) Whole-cell voltage-clamp recordings from a MC at 0 mV and –70 mV showing IPSCs (top) and EPSCs (bottom) with raphe fiber activation. Blue bars depict the timing of ChR2 fiber stimulation. (**e**) Ratio of integrated excitatory-to-inhibitory charge transfer in TCs and MCs ($n = 6$ each) following optogenetic stimulation of raphe fibers. Center line depicts the median, the edges of the box show 25th and 75th percentiles and whiskers show the extreme data points. (**f**) Scatter plots comparing the firing rate of MCs for different step current injection with and without raphe fiber activation in the presence of 5-HT receptor antagonist (50 μM methysergide, $P = 1.1 \times 10^{-19}$, Wilcoxon rank-sum test, $n = 5$ cells from 3 animals), glutamate receptor antagonists (20 μM CNQX and 50 μM AP5, $P = 7.2 \times 10^{-31}$, Wilcoxon rank-sum test, $n = 5$ cells from 4 animals) and GABA antagonist (20 μM gabazine, $P = 8.79 \times 10^{-3}$, Wilcoxon rank-sum test, $n = 5$ cells from 4 animals). (**g**) Average light-triggered changes in firing rates of all MCs averaged across different levels of current injections. The changes for different pharmacological manipulations were normalized to the condition with ACSF only. $^{*}P < 0.05$, $^{**}P < 0.01$ and $^{***}P < 0.001$. Error bars represent s.e.m.

rate for each MC, but the crossover point, where modulation shifted from inhibition to excitation or vice versa, varied from cell to cell (**Fig. 6b**). This complexity and lack of predictability of MC modulation may be attributable to network effects and the increased lateral inhibition on MCs as compared to TCs, and perhaps also to the cell to cell variability in 5-HT receptor expression (**Supplementary Fig. 1**). In summary, unlike TCs, whose firing rates were potentiated by raphe inputs, MCs had firing rates that were bidirectionally modulated, as was documented *in vivo*.

External tufted cells receive fast inputs from raphe axons

Although MCs and TCs both exhibited fast effects from raphe axon activation, the timing of the light-evoked currents strongly suggested polysynaptic pathways for these effects (**Figs. 5b** and **6d**). Therefore, we sought to identify the cell type in the OB that receives direct synaptic inputs from raphe terminals and could account for the excitatory effects recorded in MCs and TCs. We hypothesized that these recipients could be external tufted cells (ETCs), which reside at the base of the glomerular layer and possess a single dendrite that projects into a nearby glomerulus (**Fig. 7a**). ETCs receive direct inputs from OSNs and release glutamate to excite MCs and TCs at the same glomerulus[35,36]. Moreover, ETCs express 5-HT receptors and have been shown to be sensitive to pharmacological application of 5-HT[25,26]. In addition, the glomerular layer has denser innervation of raphe axons (**Supplementary Fig. 5**) than other layers in the olfactory bulb[23].

Whole-cell recordings from ETCs (**Fig. 7a**) revealed light-activated excitatory postsynaptic currents (EPSCs) aligned closely with each light pulse (**Fig. 7b**,**c**; see Online Methods). Light-evoked

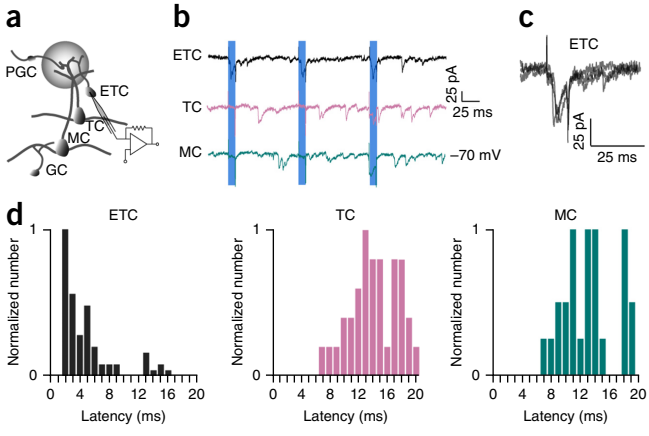

Figure 7 ETCs receive direct excitatory inputs from raphe fibers. (**a**) Diagram depicting ETC recordings from OB slices. (**b**) Whole-cell voltage-clamp recordings from at –70 mV showing short latency EPSCs in an ETC (top) and long latencies in a TC (middle) and MC (bottom). Timing of light stimulus is shown in blue. (**c**) Four successive trials from an ETC, showing short latency EPSCs at –70 mV for raphe fiber activation. (**d**) Histograms showing the latencies of EPSCs in ETCs (gray, $n = 10$ cells), TCs (purple, $n = 8$) and MCs (teal green, $n = 6$) in response to optogenetic activation of raphe fibers ($P = 3.2 \times 10^{-17}$ and $P = 2.4 \times 10^{-20}$ for TC and MC respectively, Wilcoxon rank-sum test).

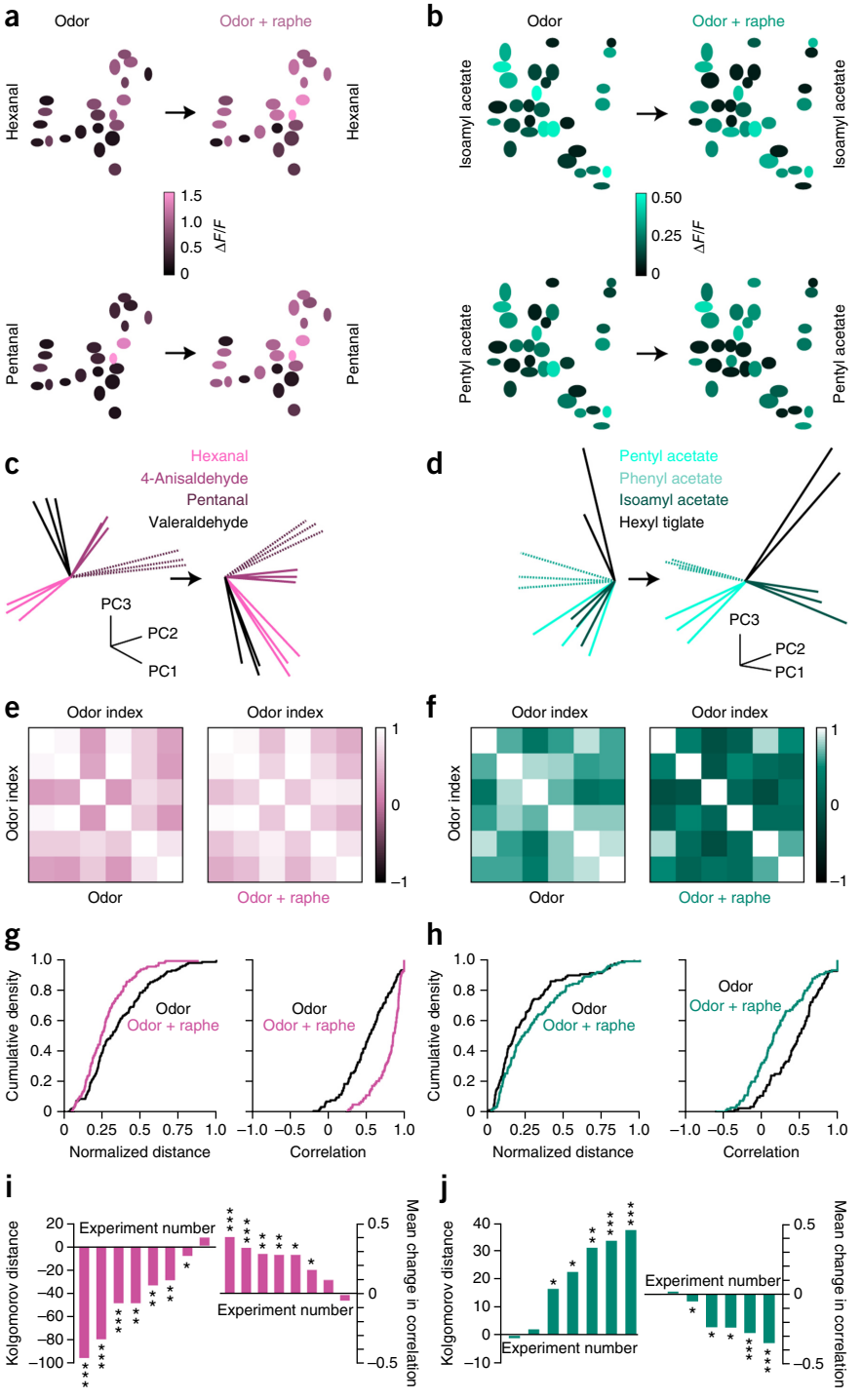

Figure 8 Raphe activation leads to sensitization of TC odor responses and decorrelation of MC odor responses. (**a**) Pseudocolor plot showing the pattern of odor responses in a region of interest for *in vivo* experiment with TCs for two odors without (left) and with (right) raphe activation. Ellipses denote individual cell bodies. (**b**) Similar plot for MC population from a different experiment. (**c**) Principal component projections of TC responses from one experiment in the space of the first three components, for four different odors without and with raphe activation. (**d**) Principal component projections for MC responses in a different experiment. (**e**) Matrix showing the correlation between odor responses of TCs (six odors) without (left) and with (right) raphe stimulation ($P = 2.16 \times 10^{-7}$, Wilcoxon rank-sum test, $n = 6$ odors). Diagonal elements have a value of 1 by definition. (**f**) Analogous matrix for MCs ($P = 7.8 \times 10^{-4}$, Wilcoxon rank-sum test, $n = 6$ odors). (**g**) Cumulative density plots comparing the inter-odor distances measured in PCA space (left) and through direct correlation between different odors (right) for the TC experiment shown in **a** and **c**. (**h**) Analogous density plots for MC experiment illustrated in **b** and **d**. (**i**) Bar graphs depicting change in the inter-odor separation for TC population when raphe is stimulated for eight separate experiments ($P < 0.05$, Wilcoxon rank-sum test, $n = 8$ animals. The change was calculated as the Kolmogorov distance between the cumulative density plots in PCA space (left) and as change in the correlation (right). (**j**) Bar graphs depicting change in the inter-odor separation for MC population when raphe is stimulated for seven separate experiments ($P < 0.05$, Wilcoxon rank-sum test, $n = 7$ animals; see Online Methods). $^{*}P < 0.05$, $^{**}P < 0.01$ and $^{***}P < 0.001$.

EPSCs were blocked by AP5 and CNQX (data not shown), indicating that they are glutamatergic. The EPSCs were reliable (8% failure rate) and had an average latency of 4.39 ± 0.39 ms (median latency of 3.1 ms) after the onset of blue light (**Fig. 7b**,**d**). This timing is congruent with monosynaptic input from raphe axons onto ETCs and is similar to that of OSNs[35,36]. By contrast, the latencies of responses in TCs (14.49 ± 0.49 ms and median of 13.3 ms, $P = 3.2 \times 10^{-17}$ for 5 animals, Wilcoxon rank-sum) and MCs (15.26 ± 0.53 ms and median of 13.6 ms) were substantially longer ($P = 2.4 \times 10^{-20}$ for 3 animals, Wilcoxon rank-sum test, **Fig. 7b**,**d**). These data suggest that ETCs receive direct excitatory, glutamatergic input from raphe axons and that they, in turn, activate glomerular networks, leading to the excitatory and inhibitory currents observed in TCs and MCs.

Raphe inputs differentially affect MC and TC coding

The OB is the first station in the brain for olfactory processing, and ensembles of MCs and TCs send different odor information from the OB to different regions of the brain[19,22]. Given that both TCs and MCs are strongly modulated by brief activation of raphe projections, we next explored how the raphe-mediated modulation of odor responses influences the coding strategies of these cells.

One potential way to enhance the discriminability of different odors by the downstream circuit is to increase the linear separability of patterns of activity of the bulbar output neurons[37]. To elucidate the changes in separability, we performed an unbiased analysis of correlations across odors using principal component analysis (PCA). For each of our *in vivo* calcium imaging experiments in which at least three odors were used (eight imaged fields of view for TCs and seven for MCs), we visualized the responses for all odor trials (**Fig. 8a**,**b**) in PC space (**Fig. 8c**,**d**). We quantified the distance between odor response

profiles in PC space using a Euclidean metric (see Online Methods). We first confirmed that the distance between repeat trials for the same odor, a measure of trial-to-trial variability of population responses, did not change between the two experimental conditions (**Fig. 8c**,**d**). The mean inter-trial Euclidean distance for TC responses was similar without and with raphe stimulation (0.86 versus 0.88, $P = 0.84$, for $n = 8$ animals, Wilcoxon rank-sum test; **Fig. 8c**). Similar results were obtained for MC responses (0.74 versus 0.72, $P = 0.76$, for $n = 7$ animals, Wilcoxon rank-sum test; **Fig. 8d**), indicating that the reliability of responses was not altered by raphe stimulation for either cell type. Raphe stimulation, however, induced significant changes in the Euclidean distances between representations of different odors (**Fig. 8e**–**j**). Inter-odor separation of TC responses significantly decreased in seven of eight experiments ($P < 0.05$, Wilcoxon rank-sum test), indicating that TC odor responses became more similar with raphe activation (**Fig. 8g**,**i**). Conversely, MC odor responses moved farther apart in PC space when the raphe was activated (**Fig. 8h**,**j**). Five of seven experiments with MCs (**Fig. 8j**) showed significantly increased separation ($P < 0.05$, Wilcoxon rank-sum test). We also found that the inter-odor distances for TCs were smaller (2.86 ± 0.05 for 764 odor pair comparisons; $P = 1.31 \times 10^{-3}$, Wilcoxon rank-sum test) than those for MCs (3.54 ± 0.02 for 584 odor pair comparisons) for odor stimulation in the absence of raphe activation, as in previous studies[31]. We obtained similar results when we used cross-correlation as a measure of similarity between the odors responses (**Fig. 8e**–**j**). With raphe stimulation, the correlation between odor responses increased for TCs ($P = 2.16 \times 10^{-7}$, Wilcoxon rank-sum test, **Fig. 8e**,**g**) and decreased for MCs ($P = 7.8 \times 10^{-4}$, Wilcoxon rank-sum test, **Fig. 8f**,**h**). This analysis indicates that raphe activation leads to increased pattern separation in MC odor codes and increased similarity of odor representation in TCs.

DISCUSSION

We have shown that raphe inputs to the OB influence odor coding on a sub-second timescale. Although TCs and MCs at rest were excited by brief activation of raphe nuclei, odor responses were generally potentiated in TCs but bidirectionally modulated in MCs. *In vitro* optogenetic experiments revealed modulation of TCs and MCs through both 5-HT and glutamate release from raphe terminals. The net effect of raphe activation was a differential modulation of TC and MC activity, with sensitization of TC odor responses and decorrelation of MC population responses to different odors.

Specificity of raphe stimulation

We ascertained the specificity of activation of raphe neurons using optogenetic methods. First, we confirmed that specific optical stimulation of serotonergic raphe neurons[33] produced effects that matched electrical stimulation of the raphe in the same M/TCs. Second, we confirmed the location of the electrode tip in all experiments. Third, direct optogenetic stimulation of raphe neurons resulted in modulation of MC and TC calcium responses that matched those produced by electrical stimulation of the raphe. Fourth, the results of our *in vivo* experiments matched the *in vitro* experiments (where specific optical stimulation was used exclusively): TC activity was always potentiated but MC activity was modulated in a bidirectional manner. These arguments strongly support the specificity of raphe stimulation.

All the data presented above were from anesthetized animals, which afforded better control, reduced variability and minimized contributions from other neuromodulatory systems. We acknowledge, however, that anesthesia alters many aspects of neuronal and synaptic function, as well as the baseline activity of raphe neurons[11]. Although extensive future studies in awake behaving animals are necessary to compare raphe modulation of OB function in different behavioral states, our preliminary experiments in awake mice have confirmed the key results on TC and MC modulation by raphe stimulation (**Supplementary Fig. 6**).

Rapid effects mediated by glutamate

Serotonergic signaling is important on timescales that vary from seconds to hours. It is implicated in the evaluation of punishment and reward on short time scales[4,5,14], control of breathing and body temperature on the time course of minutes[12] and modulation of mood and brain states on longer time scales[3,4]. Notably, brief activation of raphe neurons can drive reward behavior[5], and this fast reward signal appears to be primarily glutamatergic. Slightly longer duration activation can promote patience in subjects[7,38]. Our current results indicate that brief activation of raphe neurons has robust and diverse effects on early olfactory processing.

Activation of raphe axons led to excitation in principal neurons in the OB, as well as delayed inhibition. Excitation in ETCs occurred at short latencies and was abolished by ionotropic glutamate receptor blockers, suggesting direct release of glutamate from raphe terminals. By contrast, most of the excitation seen in TCs and MCs was delayed and asynchronous, indicative of recurrent excitation within the OB. Previous studies have shown that ETCs excite TCs and MCs through dendritic release of glutamate[35,36], offering a plausible mechanism of polysynaptic excitation. 5-HT positive axons have been shown to synapse onto both GABAergic and non-GABAergic targets in the glomerular layer[39]. Inhibitory currents activated by raphe stimulation were also polysynaptic, since they were blocked by glutamatergic blockers. Depolarization of ETCs, and subsequently of TCs and MCs, will likely recruit glomerular layer interneurons and granule cells[19], which can induce GABAergic currents in principal cells. Whether interneurons are directly excited by raphe axons must await future experiments. The net result of the dual effects on the firing rates of TCs and MCs was complex and is discussed below.

Dual release of 5-HT and glutamate by raphe axons

A key inference from our findings is the dual release of glutamate and 5-HT from raphe terminals. We found evidence for release of 5-HT with brief activation: in both TCs and MCs, methysergide led to a reduction in light-activated inhibition, suggesting that 5-HT had a net inhibitory action on principal neurons. Whether this action is due to direct inhibition through 5-HT1 receptors on principal neurons (**Supplementary Fig. 1**) or through excitation of 5-HT2 receptors on interneurons[25,26] remains to be studied. Since the effects of raphe axon stimulation were more strongly modulated by glutamatergic blockers, we predict that only modest release of 5-HT is triggered by our brief stimulation.

Previous studies have shown that many of the 5-HT-producing neurons of the raphe also express VGluT3, a vesicular glutamate transporter[5,40–43], which has been detected ultrastructurally in identified serotonergic axons[17]. Glutamate release from raphe fibers was shown to be involved in raphe modulation of behavior[5,42] and hippocampal activity[18]. In our experiments, optogenetic activation of identified raphe axon terminals in the OB had modulatory effects due to both 5-HT and glutamate, but whether these neurotransmitters are released from the same or distinct synaptic sites and whether the relative amounts of 5-HT and glutamate released is activity dependent[5] remains unclear.

This interplay between glutamate release and 5-HT release could bridge the gap between sensing/behavior and mood/state of being.

Recent studies have shown that 5-HT modulates the OB or the analogous insect circuit at multiple sites[6,9,25,26]. Previously, our laboratory showed that 5-HT activates inhibitory periglomerular cells in the glomerular layer of the OB that then inhibit incoming olfactory sensory axons, resulting in presynaptic inhibition[9]. In these earlier experiments, the raphe was activated for many minutes and 5-HT receptor antagonists blocked the effect, whereas in the experiments described here brief raphe stimulation did not alter glomerular input (**Supplementary Fig. 4**). These differences indicate that the modulatory effects of raphe projections are dependent on the timescale and degree of activity. Notably, the rapid effects of raphe activation on TCs and MCs are similar to the actions of cortical feedback to the OB[44], blurring the distinction between neuromodulation and ongoing computation.

Differential modulation of TCs and MCs

An unexpected finding from our experiments is that MCs and TCs were differentially modulated by brief activation of raphe inputs. MCs and TCs are the two main types of principal neurons in the OB, and they differ both anatomically and functionally. Their somata reside in different layers of the olfactory bulb circuit[19], and their downstream targets also diverge[19,20,22]. TCs send axons to more anterior targets, while MCs project to both anterior and posterior olfactory cortical areas[19]. Functionally, TCs are intrinsically more excitable[45] and respond to a wider range of odors and concentrations than MCs[31,32,46].

Our experiments show that these two subtypes of cells also differ in the way they are modulated by raphe inputs. We have focused on time-averaged activity in this study, leaving open potential differences in the raphe effects on temporal dynamics of TC and MC activity. It is clear that neuromodulators are important in olfactory processing[9,47–49], but our study is, to our knowledge, the first to show that neuromodulators can differentially affect MCs and TCs. MC responses tend to be more decorrelated than those of TCs, and brief raphe inputs drove these two subtypes even farther apart: TC odor responses became more correlated while MC odor responses were further decorrelated. Although both cell types received light-triggered excitation as well as inhibition, the overall effect on TCs was invariably excitatory. This could be because excitation arrives earlier in TCs and inhibition is weaker and rarely occurs without earlier excitation. One possible circuit mechanism for this effect might be weaker lateral inhibition on TCs, with most inhibition arising from the intraglomerular circuits. By contrast, each MC appeared to receive a distinct balance of excitation and inhibition, such that the net effect of firing could be in either direction. Perhaps MC inhibition can also occur without much excitation as a result of more robust interglomerular lateral connections. Interestingly, different raphe nuclei may preferentially target distinct layers of the OB[24], offering another potential source of differential effects on OB neurons.

This differential modulation of TCs and MCs may be behaviorally relevant for animals to both detect and identify stimuli. The sensitization of TCs may lead to more efficient detection of behaviorally relevant stimuli in anterior olfactory cortex, while the decorrelation of MC representation could lead to increased accuracy in identification of odors in more distal cortical areas. The synergy of these two modulatory effects could lead to improved encoding of the olfactory world.

METHODS

Methods and any associated references are available in the online version of the paper.

Note: Any Supplementary Information and Source Data files are available in the online version of the paper.

ACKNOWLEDGMENTS

We thank the members of Murthy and Dulac labs for discussions throughout the project, and D. Gire, J. Cohen and M. Thanawala for comments on the manuscript. This work was supported by research grants (DC011291 and DC014453) from the US National Institutes of Health (V.N.M.), a seed grant from the Harvard Brain Initiative (V.N.M.) and fellowships from the US National Science Foundation and the Mortimer and Theresa Sackler Foundation (A.C.P.).

AUTHOR CONTRIBUTIONS

A.C.P., V.K. and V.N.M. designed the project. A.C.P. and V.K. performed *in vivo* experiments; A.C.P. and P.A. performed and analyzed histological experiments; V.K. perform *in vitro* experiments. A.C.P. and V.K. analyzed the data with V.N.M.'s guidance. V.N.M. supervised the entire project. A.C.P., V.K. and V.N.M. wrote the paper with input from P.A.

COMPETING FINANCIAL INTERESTS

The authors declare no competing financial interests.

1. Lee, S.-H. & Dan, Y. Neuromodulation of brain states. *Neuron* **76**, 209–222 (2012).
2. Marder, E. Neuromodulation of neuronal circuits: back to the future. *Neuron* **76**, 1–11 (2012).
3. Cools, R., Roberts, A.C. & Robbins, T.W. Serotoninergic regulation of emotional and behavioural control processes. *Trends Cogn. Sci.* **12**, 31–40 (2008).
4. Dayan, P. & Huys, Q.J.M. Serotonin in affective control. *Annu. Rev. Neurosci.* **32**, 95–126 (2009).
5. Liu, Z. *et al.* Dorsal raphe neurons signal reward through 5-HT and glutamate. *Neuron* **81**, 1360–1374 (2014).
6. Dacks, A.M., Green, D.S., Root, C.M., Nighorn, A.J. & Wang, J.W. Serotonin modulates olfactory processing in the antennal lobe of *Drosophila*. *J. Neurogenet.* **23**, 366–377 (2009).
7. Fonseca, M.S., Murakami, M. & Mainen, Z.F. Activation of dorsal raphe serotonergic neurons promotes waiting but is not reinforcing. *Curr. Biol.* **25**, 306–315 (2015).
8. Hurley, L.M., Devilbiss, D.M. & Waterhouse, B.D. A matter of focus: monoaminergic modulation of stimulus coding in mammalian sensory networks. *Curr. Opin. Neurobiol.* **14**, 488–495 (2004).
9. Petzold, G.C., Hagiwara, A. & Murthy, V.N. Serotonergic modulation of odor input to the mammalian olfactory bulb. *Nat. Neurosci.* **12**, 784–791 (2009).
10. Hilaire, G. *et al.* The role of serotonin in respiratory function and dysfunction. *Respir. Physiol. Neurobiol.* **174**, 76–88 (2010).
11. Jacobs, B.L. & Azmitia, E.C. Structure and function of the brain serotonin system. *Physiol. Rev.* **72**, 165–229 (1992).
12. Ray, R.S. *et al.* Impaired respiratory and body temperature control upon acute serotonergic neuron inhibition. *Science* **333**, 637–642 (2011).
13. Hannon, J. & Hoyer, D. Molecular biology of 5-HT receptors. *Behav. Brain Res.* **195**, 198–213 (2008).
14. Cohen, J.Y., Amoroso, M.W. & Uchida, N. Serotonergic neurons signal reward and punishment on multiple timescales. *Elife* **4**, e06346 (2015).
15. Ranade, S.P. & Mainen, Z.F. Transient firing of dorsal raphe neurons encodes diverse and specific sensory, motor, and reward events. *J. Neurophysiol.* **102**, 3026–3037 (2009).
16. Rhoades, R.W., Bennett-Clarke, C.A., Shi, M.Y. & Mooney, R.D. Effects of 5-HT on thalamocortical synaptic transmission in the developing rat. *J. Neurophysiol.* **72**, 2438–2450 (1994).
17. Suzuki, Y., Kiyokage, E., Sohn, J., Hioki, H. & Toida, K. Structural basis for serotonergic regulation of neural circuits in the mouse olfactory bulb. *J. Comp. Neurol.* **523**, 262–280 (2015).
18. Varga, V. *et al.* Fast synaptic subcortical control of hippocampal circuits. *Science* **326**, 449–453 (2009).
19. Nagayama, S., Homma, R. & Imamura, F. Neuronal organization of olfactory bulb circuits. *Front. Neural Circuits* **8**, 98 (2014).
20. Haberly, L.B. Parallel-distributed processing in olfactory cortex: new insights from morphological and physiological analysis of neuronal circuitry. *Chem. Senses* **26**, 551–576 (2001).
21. Fukunaga, I., Berning, M., Kollo, M., Schmaltz, A. & Schaefer, A.T. Two distinct channels of olfactory bulb output. *Neuron* **75**, 320–329 (2012).
22. Giessel, A.J. & Datta, S.R. Olfactory maps, circuits and computations. *Curr. Opin. Neurobiol.* **24**, 120–132 (2014).
23. McLean, J.H. & Shipley, M.T. Serotonergic afferents to the rat olfactory bulb: I. Origins and laminar specificity of serotonergic inputs in the adult rat. *J. Neurosci.* **7**, 3016–3028 (1987).
24. Steinfeld, R., Herb, J.T., Sprengel, R., Schaefer, A.T. & Fukunaga, I. Divergent innervation of the olfactory bulb by distinct raphe nuclei. *J. Comp. Neurol.* **523**, 805–813 (2015).
25. Liu, S., Aungst, J.L., Puche, A.C. & Shipley, M.T. Serotonin modulates the population activity profile of olfactory bulb external tufted cells. *J. Neurophysiol.* **107**, 473–483 (2012).

26. Hardy, A., Palouzier-Paulignan, B., Duchamp, A., Royet, J.-P. & Duchamp-Viret, P. 5-Hydroxytryptamine action in the rat olfactory bulb: *in vitro* electrophysiological patch-clamp recordings of juxtaglomerular and mitral cells. *Neuroscience* **131**, 717–731 (2005).
27. Nakamura, K., Matsumoto, M. & Hikosaka, O. Reward-dependent modulation of neuronal activity in the primate dorsal raphe nucleus. *J. Neurosci.* **28**, 5331–5343 (2008).
28. Chen, T.-W. *et al.* Ultrasensitive fluorescent proteins for imaging neuronal activity. *Nature* **499**, 295–300 (2013).
29. Haddad, R. *et al.* Olfactory cortical neurons read out a relative time code in the olfactory bulb. *Nat. Neurosci.* **16**, 949–957 (2013).
30. Wachowiak, M. All in a sniff: olfaction as a model for active sensing. *Neuron* **71**, 962–973 (2011).
31. Adam, Y. *et al.* Functional transformations of odor inputs in the mouse olfactory bulb. *Front. Neural Circuits* **8**, 129 (2014).
32. Kikuta, S., Fletcher, M.L., Homma, R., Yamasoba, T. & Nagayama, S. Odorant response properties of individual neurons in an olfactory glomerular module. *Neuron* **77**, 1122–1135 (2013).
33. Zhao, S. *et al.* Cell type–specific channelrhodopsin-2 transgenic mice for optogenetic dissection of neural circuitry function. *Nat. Methods* **8**, 745–752 (2011).
34. Kapoor, V. & Urban, N.N. Glomerulus-specific, long-latency activity in the olfactory bulb granule cell network. *J. Neurosci.* **26**, 11709–11719 (2006).
35. Gire, D.H. *et al.* Mitral cells in the olfactory bulb are mainly excited through a multistep signaling path. *J. Neurosci.* **32**, 2964–2975 (2012).
36. Najac, M., De Saint Jan, D., Reguero, L., Grandes, P. & Charpak, S. Monosynaptic and polysynaptic feed-forward inputs to mitral cells from olfactory sensory neurons. *J. Neurosci.* **31**, 8722–8729 (2011).
37. Friedrich, R.W. & Wiechert, M.T. Neuronal circuits and computations: pattern decorrelation in the olfactory bulb. *FEBS Lett.* **588**, 2504–2513 (2014).
38. Miyazaki, K.W. *et al.* Optogenetic activation of dorsal raphe serotonin neurons enhances patience for future rewards. *Curr. Biol.* **24**, 2033–2040 (2014).
39. Gracia-Llanes, F.J. *et al.* Synaptic connectivity of serotonergic axons in the olfactory glomeruli of the rat olfactory bulb. *Neuroscience* **169**, 770–780 (2010).
40. Commons, K.G. Locally collateralizing glutamate neurons in the dorsal raphe nucleus responsive to substance P contain vesicular glutamate transporter 3 (VGLUT3). *J. Chem. Neuroanat.* **38**, 273–281 (2009).
41. Fremeau, R.T. Jr., Voglmaier, S., Seal, R.P. & Edwards, R.H. VGLUTs define subsets of excitatory neurons and suggest novel roles for glutamate. *Trends Neurosci.* **27**, 98–103 (2004).
42. Qi, J. *et al.* A glutamatergic reward input from the dorsal raphe to ventral tegmental area dopamine neurons. *Nat. Commun.* **5**, 5390 (2014).
43. Okaty, B.W. *et al.* Multi-scale molecular deconstruction of the serotonin neuron system. *Neuron.* **88**, 774–791 (2015).
44. Otazu, G.H., Chae, H., Davis, M.B. & Albeanu, D.F. Cortical feedback decorrelates olfactory bulb output in awake mice. *Neuron* **86**, 1461–1477 (2015).
45. Burton, S.D. & Urban, N.N. Greater excitability and firing irregularity of tufted cells underlies distinct afferent-evoked activity of olfactory bulb mitral and tufted cells. *J. Physiol. (Lond.)* **592**, 2097–2118 (2014).
46. Scott, J.W. Electrophysiological identification of mitral and tufted cells and distributions of their axons in olfactory system of the rat. *J. Neurophysiol.* **46**, 918–931 (1981).
47. Kiselycznyk, C.L., Zhang, S. & Linster, C. Role of centrifugal projections to the olfactory bulb in olfactory processing. *Learn. Mem.* **13**, 575–579 (2006).
48. Rothermel, M., Carey, R.M., Puche, A., Shipley, M.T. & Wachowiak, M. Cholinergic inputs from Basal forebrain add an excitatory bias to odor coding in the olfactory bulb. *J. Neurosci.* **34**, 4654–4664 (2014).
49. Shea, S.D., Katz, L.C. & Mooney, R. Noradrenergic induction of odor-specific neural habituation and olfactory memories. *J. Neurosci.* **28**, 10711–10719 (2008).

ONLINE METHODS

***In vivo* imaging experiments.** All procedures were performed using approved protocols in accordance with institutional (Harvard University Institutional Animal Care and Use Committee) and national guidelines. For *in vivo* two-photon imaging experiments, Tbx21-Cre mice were used[29]. Mice (age 2–6 months) were anesthetized with a mixture of ketamine (100 mg/kg) and xylazine (10 mg/kg) and placed in a stereotaxic apparatus in accordance with Harvard University animal welfare guidelines. A small craniotomy was performed over each olfactory bulb (OB) and 200 nL of AAV2.9 virus (UPenn Vector Core) carrying flex GCaMP6s (ref. 50) was injected 1 mm deep in each OB through a glass micropipette attached to a nanoinjector (MO-10, Narishige).

Three to 6 weeks after injection, mice were anesthetized and a custom-built titanium head plate was secured to their skull with bone cement (Dentsply). A cranial window was placed 3.5 mm lateral to the lambda. A bipolar electrode (FHC) was stereotaxically placed in the raphe at a 45 degree angle, −4.25 mm posterior to the bregma, 0 medial-lateral, 3.5 mm deep. A second cranial window was placed over the OBs to expose their dorsal surface. 1.2% agarose in saline and a coverslip were placed over the second cranial window for imaging. Sterile saline was used as the fluid for the immersion objective.

For optogenetic experiments, TPH2-ChR2-YFP[33] mice were injected with nonconditional AAV GCaMP6s virus. Two to 4 weeks after injection, an optical fiber (300 μm core, Polymicro Technology) was implanted in the raphe and the fiber was coupled to a 473-nm blue DPSS laser (Laserglow Technology). The laser was shuttered using a custom-built shutter to allow timed stimulation.

For awake experiments, a custom-built bipolar electrode (0.0002-inch coated SS wire, A-M systems) was implanted in the raphe and attached to the skull via magnets (0.0625-inch disc magnets, Magcraft).

Breathing was monitored via a stress sensor (Kent Scientific) placed around the abdomen. A custom-built microscope was used for *in vivo* imaging as described previously[9]. Calcium indicators were excited and imaged (4–20 Hz) with a water immersion objective (20×, 0.95 NA, Olympus) at 927 nm using a Ti:sapphire laser (Chameleon Ultra, Coherent) with a 140-fs pulse width and 80-MHz repetition rate. Image acquisition, scanning and stimulus delivery were controlled by custom-written software in LabView (National Instruments). Odors were delivered via a custom-built olfactometer as described previously[51]. For odor trials, odors were delivered for 3 s after 5–10 s of baseline. Each odor presentation was repeated at least twice for both odor-only and odor-plus-raphe stimulation trials. Stimulation and non-stimulation trials were interleaved, and blank trials in which no odor or stimulation (clean air only) were given were also interspersed. Odors were diluted in diethyl phthalate solvent (Sigma-Aldrich) at 5% v/v; **Supplementary Figure 2** has the list of odors used. Electrical stimulation (250 μA, three 1-ms biphasic pulses at 10 Hz; negative peak first; SD9 Grass) of the raphe began 1 s after odor onset. Electrical stimulation signals were recorded for each stimulation trial to ensure timing and current amplitude. In baseline excitation trials, stimulation was initiated 5–10 s after trial onset. As with the odor trials, non-stimulation and stimulation trials were interleaved, with stimulation trials repeated at least three times.

At the termination of the experiment, an electrolytic lesion (10 s, square pulse, 5 mA) was made to check the position of the bipolar electrode in the raphe. Mice were transcardially perfused and the brains removed from the skull. Coronal floating sections were cut using a vibratome (Leica VT1000S). Only mice with a clear lesion ventral to the central aqueduct were included in the data analysis. Although the electrolytic lesion was clear in the floating sections, some sections were mounted and Nissl staining was performed. Sections were dried overnight, followed by staining with filtered cresyl violet blue solution (500 ml distilled water, 2.5 g cresyl violet acetate, 1.5 ml glacial acetic acid). They were then dehydrated using a series of ethanol dilutions (50%, 60%, 80%, 90%, 95% and 100%), cleared with xylenes and coverslipped using Cytoseal 60. Slides were imaged using a Zeiss AxioImager Z2.

Identification of cells. For *in vivo* imaging experiments, we used Tbx21-Cre animal, in which Cre recombinase is selectively expressed in the principal neurons (MCs, TCs and ETCs) of the OB[29] (**Supplementary Fig. 1** and **Supplementary Movie 1**). We used depth and the cell body location within a specific layer (MCL or EPL) as a criterion to classify the cell identity. Our viral injection resulted in sparse labeling of cells in EPL and MCL (**Supplementary Fig. 1** and **Supplementary Movie 1**); cells located in the EPL were classified as TCs and the cells in the MCL were classified as MCs.

For *in vitro* slice electrophysiology experiments, we used previously well-established criteria to classify the cells. Principal neurons of the OB have significantly larger cell bodies compared to the inhibitory neuronal populations in the OB. As in previous studies, cells with >50% of the cell body lying in MCL were classified as MCs. Neurons that were entirely situated in the EPL were classified as TCs. To identify and record from ETCs, we performed cell-attached recordings from the cells with large cell bodies close to the glomerular layer, and the cells that showed rhythmic bursting were used for whole-cell patch recordings.

***In vivo* electrophysiology.** For *in vivo* electrophysiology, transgenic TPH2-ChR2-YFP mice were used[33]. For ChR2 negative controls, we used C57/B6 mice (Jax). Mice (age 2–8 months) were anesthetized, as mentioned above, with a mixture of ketamine (100 mg/kg) and xylazine (10 mg/kg) and fitted with a head plate that was secured with bone cement (Dentsply). A single cranial window was placed over one OB. MC and TC signals were recorded using tungsten electrodes (1–5 MΩ; FHC). Signals were amplified and filtered (100 Hz–1 MHz) and sampled at 20 kHz (A-M Systems). ChR2 was activated by three 10-ms blue light pulses shone on the surface of the cranial window at 10 Hz (~15 mW/mm^2). Trials were spaced by at least 15 s, and light trials were repeated 10–50 times.

Spikes with amplitudes greater than 5 times the s.d. of the baseline were sorted manually according to their projections into principal component space. We only accepted cells with at least 95% of spikes exhibiting an interspike interval greater than 3 ms. Significance of PSTHs was determined by comparing the average rate during a 5-s period following blue light activation with a corresponding period with no light using a sign test.

***In vitro* electrophysiology.** Slices were prepared using methods adapted from previous work[34]. Mice (4–12 weeks old, TpH2-ChR2-YFP) were deeply anesthetized with a mixture of ketamine (100 mg/kg) and xylazine (10 mg/kg) and then perfused with ice-cold modified ACSF solution (in mM: 120 choline chloride, 25 glucose, 25 $NaHCO_3$, 2.5 KCl, 0.5 $CaCl_2$, 10 $MgSO_4$, 5 sodium ascorbate, 3 sodium pyruvate, 1.25 NaH_2PO_4). Brains were removed and placed in the same ice-cold modified ACSF. Sagittal slices (300 μm thick) of olfactory bulbs were cut using a vibratome (VT1000S; Leica, Germany). After cutting, slices were incubated in the above-mentioned ACSF solution (continuously oxygenated) at 37 °C for 30 min before being transferred to oxygenated ACSF (in mM: 25 NaCl, 2.5 KCl, 25 $NaHCO_3$, 1.25 NaH_2PO_4, 1 $MgSO_4$, 25 glucose, 2.0 $CaCl_2$).

Whole-cell current-clamp recordings were made using patch pipettes filled with internal buffer (in mM: 120 potassium gluconate, 2.0 sodium gluconate, 10 HEPES, 4.0 Mg-ATP, 2.0 Na_2-ATP, 0.3 Na_3-GTP, 4.0 NaCl and 1% biocytin) and voltage-clamp recordings were made using internal buffer (in mM: 130 D-gluconic acid, 130 cesium hydroxide, 5.0 NaCl, 10 HEPES, 12 di-tris-phosphocreatine, 1 EGTA, 3.0 Mg-ATP, 0.2 Na_3-GTP with 1% biocytin) using a Multiclamp 700B amplifier (Molecular Devices, Palo Alto, CA). Cells were visualized under custom-built infrared optics on a BX51WI microscope (Olympus Optical, Tokyo, Japan). Physiological data were collected via software written in LabView (National Instruments) and pClamp 10.3 (Molecular Devices). All recordings were performed at 35 °C in regular oxygenated ACSF unless mentioned otherwise. Pharmacological agents, gabazine (SR 95531 hydrobromide), DL-AP5, CNQX and methysergide maleate (all from Tocris Bioscience) were added as indicated in the main text.

We used a bright light-emitting diode (LED) array (CBT-90B, Luminus Devices) with peak emission at 465 nm that was coupled to the rear lamp housing of an Olympus BX51 upright microscope, with an intensity of 6–12 mW/mm^2 in the plane of the slice[52]. Three brief pulses of blue light of 10 ms each at 10 Hz were used to activate the ChR2-positive axon fibers. Trials were spaced at least 60 s apart and stimulated (blue light) and unstimulated trials were interspersed.

To characterize the effect of light stimulation, we calculated the charge transferred as the area under the curve for the entire duration of the recording (~1.3 s) under voltage clamp (both for 0 mV and −70 mV recordings). To calculate the E/I (excitatory to inhibitory charge) ratio, we calculated the absolute change in the charge transfer for both conditions ~0 mV and −70 mV and divided them to get the unit-less number.

Data analysis. *Image analysis.* Data were analyzed with custom software (Matlab). The different frames of a given stack were first registered using a cross-correlation-based registration algorithm (dftregistration.m in Matlab).

Raw fluorescence time course was calculated from each region of interest. Fluorescence changes were expressed as a fraction of the baseline fluorescence, or $\Delta F/F_0$, where F_0 was the average fluorescence over the 5 s preceding odor onset or raphe stimulation onset, in odor and baseline trials, respectively. Average integrated odor responses were calculated over a 7-s window starting at odor onset for odor trials and stimulation onset for baseline activation trials. To determine the number of odors to which single neurons responded, we used a threshold value of 3.0 × the s.d. of the same 7 s from blank (no odor, no stimulation) trials, and the same criterion was also used to determine the number of cells that showed significant modulation in their responses.

Regression analysis. We performed the following single-variable or multi-variable regression analysis for predicting neuronal responses to the combined effect of odor and raphe stimuli.

Single-variable linear regression:

$$y = \beta_1 + \beta_2 x_1$$

where y is the predicted response of a given neuron to odor delivery in presence of raphe activation, x_1 is the response of the same neuron to either odor input or raphe stimulation, β_1 is a constant and β_2 is the weight for the odor or raphe stimulation.

Multi-variable linear regression:

$$y = \beta_1 + \beta_2 x_1 + \beta_3 x_2$$

where y is the predicted response of a given neuron to odor delivery in presence of raphe activation, x_1 is the response of the same neuron to odor stimulus, x_2 is the response of the same neuron to raphe stimulation, β_1 is a constant term, and β_2 and β_3 are weights for the odor and raphe stimulations respectively.

Interactive regression model:

$$y = \beta_1 + \beta_2 x_1 + \beta_3 x_2 + \beta_4 x_1 x_2$$

where, in addition to the terms described for the multi-variable linear regression model, we include a term for interaction between x_1 and x_2 with a weight of β_4.

In addition, residuals were calculated as the difference between the predicted values and the observed values. We also performed F-statistics on the coefficients/weights to determine if they were significant.

Distance analysis. Experiments with three or more odors were used to analyze the effect of raphe modulation on the odor-evoked population activity patterns in MCs and TCs. For every experiment, the integrated responses from the odor-only trials and those on which odor was paired with raphe activation were pooled to calculate the covariance matrix. The first three principal components (accounting for ≥90% of the variance) were used to project the individual odor responses onto a three-dimensional space. The intra-odor distance in the PCA space was calculated as the mean pairwise distance between the vectors belonging to the same odor under same conditions (odor only or odor paired with raphe activation) across different trials. In other words, we compared responses across multiple trials under equivalent conditions.

Pairwise distance was calculated as

$$d_{\text{intra}}(o) = \sqrt{\sum_{i=1}^{3} (x_i(o) - y_i(o))^2}$$

where o is odor identity and x and y are projections of individual trials for same conditions in first three principal components.

The inter-odor distance was calculated as the mean pairwise distance between the vectors for different odors under the same condition (odor alone or odor plus raphe activation), normalized by the square root of products of intra-odor distances for the odors involved.

Statistics. Non-parametric statistical tests were used. No assumption of normality of data was made. A Wilcoxon signed-rank test was used for repeated measurements of the same cell and also for the paired data sets. A Wilcoxon rank-sum test was used for comparing all unpaired non-normal distributions. Between 2 and13 animals per experiment were used. Effort was made to minimize the number of animals used and to obtain the maximum data per animal. The number of animals used and number of trials or repetitions done per animal were large enough to obtain a strong data set with statistical power and are congruent with previously published studies. F statistics were used to evaluate the goodness of fit for regression analysis. Variance within a group was described as s.e.m.

No blinding was done and subjects were not randomized, but the individual trials were randomized in a given experiment. Pseudorandom sequences were generated using Matlab and were used to control the identity of individual trials.

A **Supplementary Methods Checklist** is available.

50. Atasoy, D., Aponte, Y., Su, H.H. & Sternson, S.M. A FLEX switch targets Channelrhodopsin-2 to multiple cell types for imaging and long-range circuit mapping. *J. Neurosci.* **28**, 7025–7030 (2008).
51. Soucy, E.R., Albeanu, D.F., Fantana, A.L., Murthy, V.N. & Meister, M. Precision and diversity in an odor map on the olfactory bulb. *Nat. Neurosci.* **12**, 210–220 (2009).
52. Markopoulos, F., Rokni, D., Gire, D.H. & Murthy, V.N. Functional properties of cortical feedback projections to the olfactory bulb. *Neuron* **76**, 1175–1188 (2012).